12th CIRP Conference on
Photonic Technologies [LANE 2022]

Industrial Paper

Investigation of the influence of geometry variation on crack formation and crack controlling by a movable heating system during Laser Powder Bed Fusion

Marco Rudolf[a,*], Sebastian Edelhäuser[b], Martin Leuterer[b], Matthias Goldammer[c]

[a]*MTU Aero Engines AG, Dachauer Straße 665, 80955 Munich, Germany*
[b]*EOS GmbH, Robert-Stirling-Ring 1, 82152 Krailling / Munich, Germany*
[c]*Siemens AG, Otto-Hahn-Ring 6, 81739 Munich, Germany*

Abstract

A vane segment sample made of the alloy MAR-M247LC which is prone to hot cracking, was built by laser powder bed fusion with a newly applied movable induction heating system. The selected vane segment represents changing part structures from thin to thick which is a well-known challenge in Additive Manufacturing in combination with highly focused energy input by the laser beam and the resulting inhomogeneous thermal stresses.
This study investigated the applied heating system and its capability to reduce crack formation as well as the γ'-phase formation of difficult-to-weld nickel-based-superalloys.
The results showed that the heating system cannot entirely compensate the thermal stress within the vane segment caused by part geometry variation. A high crack formation in dependency on the thin and thick part structure as well as small γ'-precipitates due to high cooling rates were identified.

© 2022 The Authors. Published by Bayerisches Laserzentrum GmbH

Keywords: Laser powder bed fusion; MAR-M247LC; part geometry variation; movable induction heating system; cooling rate; nickel-based-superalloys

1. Introduction

Difficult-to-weld γ'-precipitation hardened nickel-based superalloys are prone to hot cracking during the manufacturing by laser welding as well as laser powder bed fusion (L-PBF) (Ojo et. al, 2003), (DuPont et. al., 2009), which can be partially adjusted and reduced by adequate process parameterization (Carter, 2013). One of the most critical crack mechanisms is known as solidification cracking and characterized by a presence of a liquid film during the solidification process. A crack-reduced part production out of these alloys can be supported by using an appropriate substrate temperature between 950 °C to 1,200 °C in the process area of the L-PBF during the melting process (Bidron et. al., 2020), (Hagedorn et. al., 2013), (Risse, 2019).

Current heating systems for L-PBF and laser welding apply a global heating approach by inductive or conventional heating devices which heats up the entire part to a consistent process temperature in-situ during the full building process. This approach has several disadvantages regarding crack formation:

- A variation in part geometry changes the temperature distribution which cannot be compensated by the fixed global heating system (Álvarez Tejedor et. al., 2013)
- The in-situ heat treatment during the several hours lasting built process caused by the global heating approach leads to an excessive growth of the γ'-precipitates that has a negative impact on the mechanical part properties (Bidron et. al., 2020), (Hagedorn et. al., 2013), (Álvarez Tejedor et. al., 2013)
- A continuous change of the thermal boundary conditions by the layer-wise building process of the L-PBF (Risse, 2019)

* Corresponding author. Tel.: +49 89 1489 6989.
E-mail address: marco.rudolf@mtu.de

© 2022 The Authors. Published by Bayerisches Laserzentrum GmbH

The examined solution is the development of a moving inductive heating system, locally linked to the position of the laser process area regardless of the respective part geometry. It has also additional benefits regarding the mechanical and thermal design of the L-PBF system in contrast to heating approaches that heat the entire system up to temperatures above 950 °C. This heating system achieves the required substrate temperature locally and can continuously ensure a homogenous temperature distribution for the laser-powder interaction area.

2. Experimental setup

2.1. Concept of the movable induction heating system

The original structure of the heating system is based on the principle described in the patent of Jakimov et. al., (2013). Fig. 1a) shows the heating concept with two inductors as well as their possible motion directions. The induction system was mounted in a modified process chamber of an EOS-M290-machine manufactured by EOS GmbH. Both inductors are positioned closely above the building area to ensure maximum energy transfer by the heating system. The outer inductor - operated at mid frequency (MF-inductor) - covers the usable building area in y-direction and is movable in x-direction. Simultaneously, the inner inductor – powered by a high frequency electrical current (HF-inductor) – is movable together with the MF-inductor in x- and individually in y-direction. Both inductors can reach any position in the x-y-plane and can consider any part geometry, which is variable over the course of the manufacturing process – even in z-direction. The MF-inductor keeps adjacent parts also at an elevated temperature (see Fig. 1a), while the process area within the HF-inductor represents the moving working area of the laser beam and process temperature monitoring which is shown in Fig. 1b).

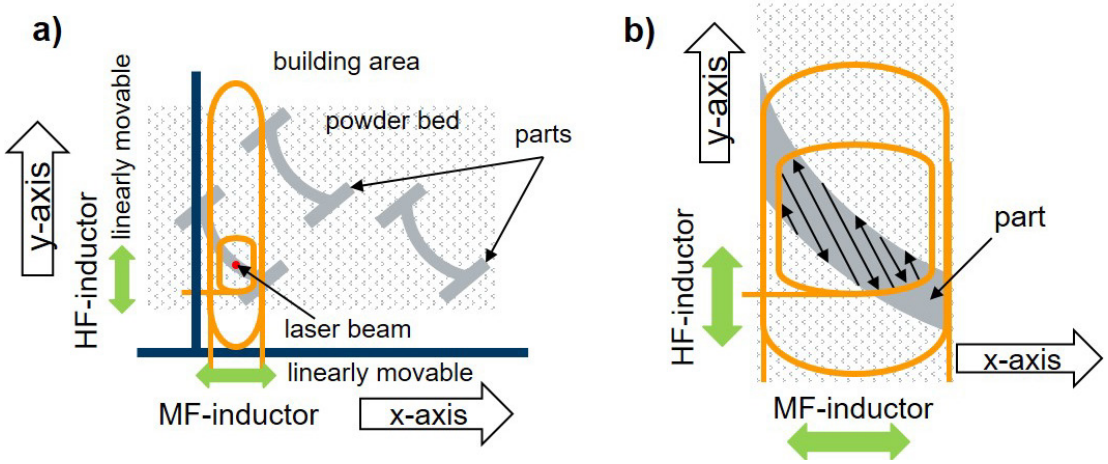

Fig. 1. Schematic representation of a) the movable induction heating system and b) detailed demonstration of the working area within the HF-inductor

2.2. Representative part geometry and parameters of the building process

γ‘-precipitation hardened nickel-based superalloys are mainly used for the hot gas path of turbines. As a test geometry - representative for this application - a vane segment was selected. This vane segment consists of a thin structure with a variable cross-section embedded between two solid blocks. The geometry demands an advanced heating concept and control for maintaining the required heating temperature before, during, and after the laser exposure for each section of the layer built-up by L-PBF.

The vane segment was made of the alloy MAR-M247LC. It was built on a cuboid Inconel 718® preform and consisted of 500 layers built with a layer thickness of 40 µm. The parameters are defined based on an established reference parameter combination at a heating temperature of 1050 °C with a volume energy of 50 J/mm³. This enabled the additive manufacturing of the vane segment. A conventional stripe scanning strategy was used.

3. Results

Fig 2a) shows the built vane segment as well as the planes S1 and S2 of the cross-section used for the metallographic examination. Microsection S1 (Fig 2b) represents the y-z-plane, while microsection S2 (Fig 2c) represents the x-y-plane; this leads to a cross-cut parallel and a perpendicular one to the building direction of the part. Both microsections have been analyzed by scanning electron microscopy (SEM) to determine potentially available cracks as well as their classification. As visible in microsection S1 and S2, the part geometry and therefore the volume of the part changes both - in building direction and within one building layer. Microsection S1 shows the crack formation with cracks through the base of the vane segment. In the blade element itself no

cracks are visible, expect one lack of fusion defect closely located to the base of the segment which was not the subject of this investigation. The maximum measured length of a single crack was approx. 873 µm (marked in Fig 2b). A detailed view of this crack, by a magnification of 3,000x, is visible in Fig 2d). An energy dispersive x-ray (EDX) analysis was additionally performed on this crack to investigate the distribution of single alloy elements, in particular regarding irregular segregations of high-dense elements like Wolfram or Hafnium. The distribution of these elements was inconspicuous.

Fig 2c) shows the crack formation in microsection S2 with cracks through the entire lateral block. These are connected by further fine cracks to a network across the width of the block. In the transition area towards the blade element no cracks are visible.

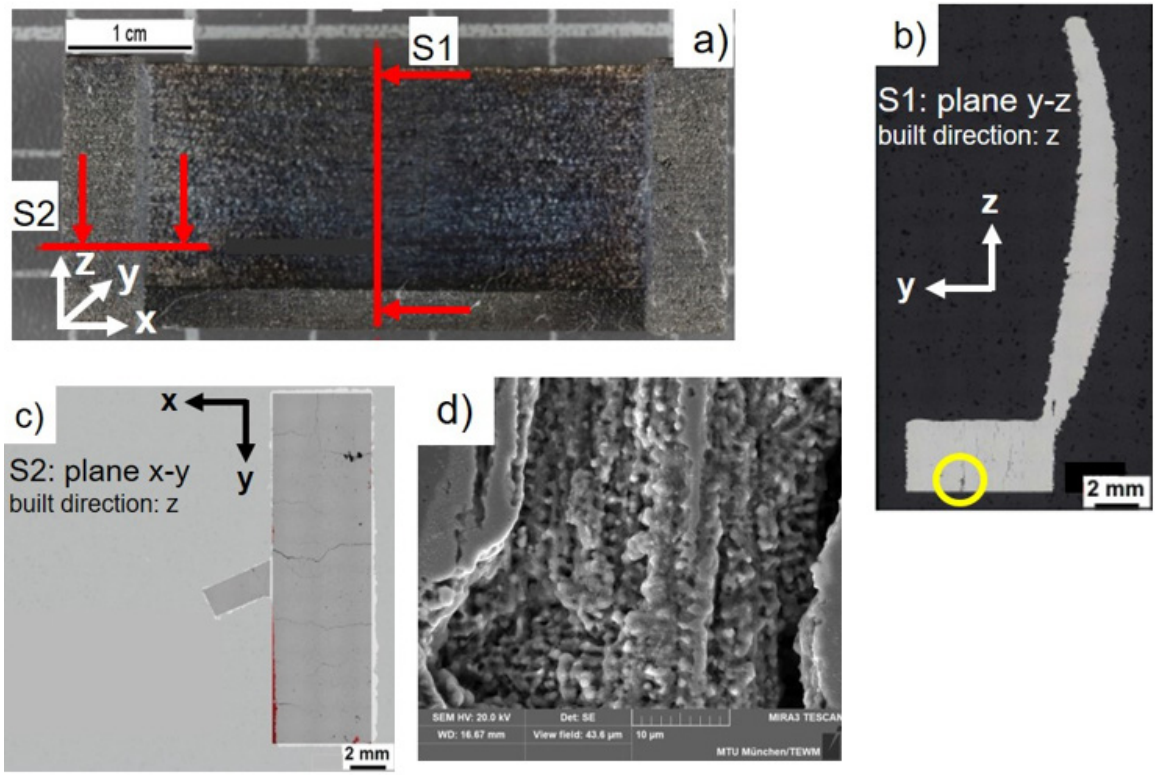

Fig 2. Representation of the built vane segment, a) including the schematic microsection S1 (plane x-z) and S2 (plane x-y) in the as built part, b) metallographic microsection S1, c) metallographic microsection S2 and d) magnification of the marked crack in microsection S1. Building direction in z-direction for all figures.

Fig 3a) shows again the metallographic microsection S1 to specify the location of the further γ- and γ'-inspection. In Fig 3b) the microsection and the phase-distribution of the marked area of Fig 3a) is visible, at a magnification of 20,000x. While Fig 3c) shows the occurred phases of the marked area in Fig 3b) at a high resolution with a magnification of 50,000x. The area-percentage of γ'-precipitates was determined, for three locations within the marked area of microsection S1 (Fig 3a), as 49.1 (± 2.65) % in average by a mean size of the γ'-precipitates of 0.16 (± 0.11) µm.

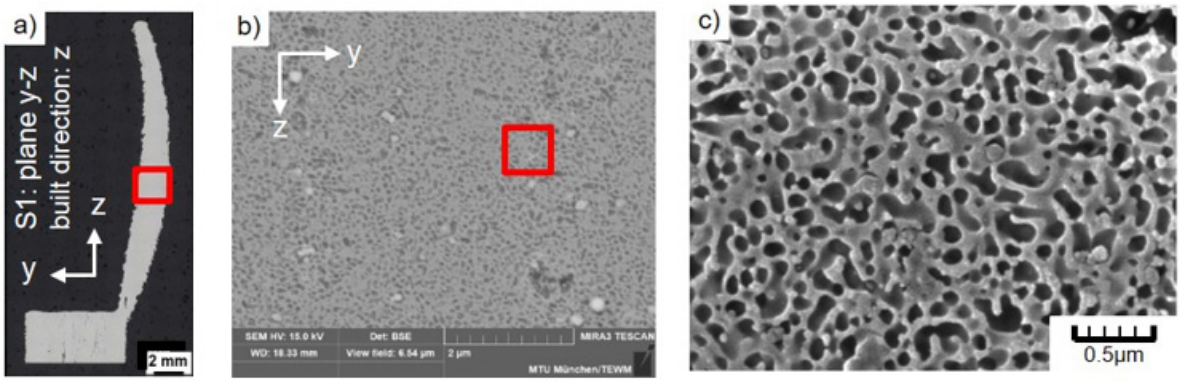

Fig 3. Microsection S1 with a) the area (red square) of the γ- and γ'- inspection, b) γ- and γ'- phases-distribution at a magnification of 20,000x and c) high detail resolution of a local area of figure b) at a magnification of 50,000x

4. Discussion

The SEM microscopy (Fig 2d) of the longitudinal cross-section S1 (Fig 2b) detected conspicuous solidification structures within the crack surface. According to Ojo et. Al (2003), these occur preferentially in full austenitic alloys like MAR-M247LC next to interdendritic areas, due to their high amount of the elements niobium as well as titanium. Furthermore, the dendrite structure within the crack indicates a nearly complete solidification process which prevents the replenishment of existing liquid proportion by Carter (2013), visible at the surface structure.

The interaction of the local heating up to the adequate temperature, the inductor placement, the energy input by the laser, as well as the concept related local cooling as the inductors move on lead to a periodically passing through the γ‘-precipitation temperature interval. The range is specified between 850 °C and 1,160 °C by Álvarez Tejedor et. al. (2013) as well as Smashey et. al. (1999). In addition, due to the heating concept, there are part areas outside the respective process zone during the laser exposure, which showed a substrate temperature below 850 °C, so that less γ‘-precipitates dissolved. This encourages the mechanism of strain age cracking by increasing the internal stresses through the uncontrolled γ‘-precipitation.

The created γ‘-precipitate of the regarded vane segment had an average size of 0.16 µm. For comparison, the γ‘-precipitate in the studies of Bidron et. al. (2020) and Hagedorn et. al. (2013) had approx. 0.5 µm at a substrate temperature of 1,100 °C, respectively a maximum size of approx. 1 µm by a temperature of 1,200 °C. Both investigations used a global heating approach. The above described interaction of the applied heating system increases the cooling rates locally and lead to the small γ‘-precipitates compared to coarse γ‘-precipitates of slow cooling rates by Bidron et. al. (2020) and Hagedorn et. al. (2013).

In addition, the changing geometry of the part, the induction-immanent effects, including the size and position of the inductors, in contrast to the part dimensions and in combination with the L-PBF specific scan strategy lead to increased temperature gradients within the part volume and thereby also to irregular local cooling rates (Adegoke et. al., 2020).

Opposed to the base of the vane segment or the lateral blocks, within the blade structure no cracks were detectable (cf. Fig 2b and Fig 2c). This specific part geometry enables a more stable temperature control of the local heating system due to the improved aspect ratio of the effective heating area and the part volume below. This ensures small cooling rates of the process area. Additionally, by Adegoke et. al. (2020) and Zhang et. al. (2019), the surrounding metal powder serves as an isolator and maintains a highly homogenous part temperature.

Taking these findings into account, we do have to distinguish between bulky part areas with a strong tendency of crack formation and the crack-free filigree part areas. The applied heating system shows a high dependency on the part geometry and could not control the cooling rates sufficiently to reduce crack formation in MAR-M247LC within a suitable range for bulky part areas.

Acknowledgement

The authors gratefully acknowledge the support of the “Bundesministerium für Bildung und Forschung” within the research project “Integrierte photonische Prozessketten für beschleunigte Produktinnovationen - GenChain” (research project 13N13593). The authors also acknowledge the support by the members of the project working group.

References

Adegoke, O., Andersson, J., Brodin, H., Peterson, R., 2020. Review of Laser Powder Bed Fusion of Gamma-Prime-Strengthened Nickel-Based Superalloys. Metals - Open Access Metallurgy Journal Volume 10, 1-26

Álvarez Tejedor, T., Generación, E., Singh, R., Pilidis, P., 2013. Maintenance and repair of gas turbine components, in “Modern gas turbine systems - High efficiency, low emission, fuel flexible power generation”. In: Jansohn, P. (Ed.). Woodhead Publishing Limited, Cambridge, 565-631

Bidron, G., Doghri, A., Malot, T., Fournier-dit-Chabert, F., Thomas, M., Peyre, P., 2020. Reduction of the hot cracking sensitivity of CM-247LC superalloy processed by laser cladding using induction preheating. Journal of Materials Processing Technology, 1-9

Carter, L., 2013. Selective Laser Melting of Nickel Superalloys for high Temperature Applications. PhD Thesis, University of Birmingham.

DuPont, J. N., Lippold, J. C., Kiser, S. D., 2009. Welding metallurgy and weldability of Nickel-Base Alloys, John Wiley & Sons, pp. 207-254.

Hagedorn, Y.-C., Risse, J., Meiners, W., Pirch, N., Wissenbach, K., 2013. Processing of nickel based superalloys MAR M-247 by means of High Temperature Selective Laser Melting (HT-SLM). High Value Manufacturing Advanced Research, 291-295.

Jakimov, A., Retze, U., Hanrieder, H., 2013. Mehrfach-Spulenanordnung für eine Vorrichtung zur generativen Herstellung von Bauteilen und entsprechendes Herstellverfahren. Patent DE102012206122A, 2013

Ojo, O. A., Richards, N. L., Chaturvedi, M. C., 2003. Contribution of constitutional liquation of gamma prime precipitate to weld HAZ cracking of cast Inconel 738 superalloy. Scripta Materialia Volume 50, 641-646

Risse, J., 2019. Additive Manufacturing of Nickel-Base Superalloy IN738LC by Laser Powder Bed Fusion. PhD Thesis, RWTH Aachen.

Smashey, R., Kelly, T., Snyder, J., Sheranko, R., 1999. Welding of Nickel-base superalloys having nil- ductility range. Patent US5897801, April 27th, 1999.

Zhang, S., Lane, B., Whiting, J., Chou, K., 2019. On thermal properties of metallic powder in laser powder bed fusion additive manufacturing. Journal of Manufacturing Processes, 382-392.